Ovonic Threshold Switching Ge_xSe_y Chalcogenide Materials: Stoichiometry, Trap Nature and Material Relaxation from First Principles

Sergiu Clima, Daniele Garbin, Karl Opsomer, Naga S. Avasarala, Wouter Devulder, Ilya Shlyakhov, Jonas Keukelier, Gabriele L. Donadio, Thomas Witters, Shreya Kundu, Bogdan Govoreanu, Ludovic Goux, Christophe Detavernier, Valeri Afanas'ev, Gouri S. Kar, Geoffrey Pourtois*

Dr. S. Clima, Dr. D. Garbin, Dr. K. Opsomer, N.S. Avasarala, Dr. W. Devulder, G. L. Donadio, T. Witters, S. Kundu, Dr. B. Govoreanu, Dr. L. Goux, Dr. G.S. Kar, Dr. G. Pourtois
imec, Kapeldreef 75, B-3001 Leuven, Belgium
E-mail: sergiu.clima@imec.be

J.Keukelier, Prof. C. Detavernier
Cocoon, Department of Solid State Sciences, University of Gent, Belgium

N.S. Avasarala, I. Shlyakhov, Prof. V. Afanas'ev
University of Leuven, Celestijnenlaan 200D, B-3001 Leuven, Belgium.

Dr. G. Pourtois
PLASMANT, University of Antwerp, 2610 Antwerpen, Belgium.
Keywords: Selector, Ovonic threshold switch, Germanium Selenide

Density Functional Theory simulations have been used to identify the structural factors that define the material properties of OTS. They show that the nature of the mobility-gap states in amorphous Ge-rich $Ge_{50}Se_{50}$ is related to Ge-Ge bonds, whereas in Se-rich $Ge_{30}Se_{70}$ – Ge valence-alternating-pairs and Se lone-pairs are dominating. To obtain a faithful description of the electronic structure, delocalization of states, it is required to combine hybrid exchange-correlation functionals with large unit-cell models. The extent of the localization of the electronic states depends on the applied external electric field. Hence, OTS materials undergo structural changes during the electrical cycling of the device, with a decrease in the population of less exothermic Ge-Ge bonds in favor of more exothermic Ge-Se. This reduces the amount of charge traps, which translates into coordination changes, increase in mobility-gap and subsequently changes the selector device electrical parameters. The threshold voltage drift process can be explained by the natural evolution of the non-preferred Ge-Ge bonds (or

"chains"/clusters thereof) in Ge-rich Ge_xSe_{1-x}. The effect of extrinsic doping is shown for the case of Si and N, which introduce strong covalent bonds in the system, increase both the mobility-gap and the crystallization temperature and decrease the leakage current.

Introduction: Newly emerging resistive memories could meet a limited set of segments of the memory class hierarchy (***Figure 1***a) due to their intrinsic limitations that cannot be easily bypassed. At first sight, the fast switching speed and much longer endurance of the resistive memories would seem to enable them as a good competitor for the NAND flash memories. However, the lack of a cost-effective 3D integration and multilevel cell design (taking into account the wide distribution of their resistance), set the resistive memories behind what can be achieved with the state-of-the-art 3D NAND FLASH memories. On the other hand, if the switching speed is meeting the DRAM requirements, the millions of endurance cycles that can be achieved are nowhere near the DRAM requirements (1E15 cycles). Therefore, another class of memories, namely the Storage Class Memory (SCM), has recently emerged to fill the gap between DRAM and FLASH. Fortunately, some current resistive memories would meet the requirements of the SCM, provided that they are associated with a performant selector device. Several types of devices/physical mechanisms can be exploited to operate a selector device (*Figure 1b*).[1]

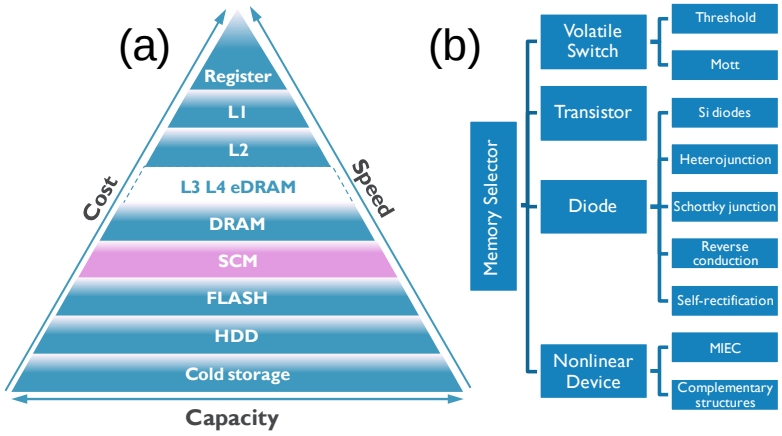

Figure 1 (a) Illustration of the gap present between DRAM and FLASH memories that is filled by the Storage-Class Memory. (b) Several device classes can be used as selector.

The most important electrical requirement for the selector device is that it should deliver a low I_{off} current at low voltages (i.e. below half the operating V_{op} for the resistive memory element), but in the same time, to be able to conduct high I_{on} at V_{op} (**Figure 2**a). When used in series with the memory device, such an element can block the parasitic leakage and allows, below a certain threshold voltage (V_{th} of the selector), the suppression of the leakage current through the half-selected neighboring ON cells. This setup allows only the fully selected cell to be read or written (Figure 2b).[2]

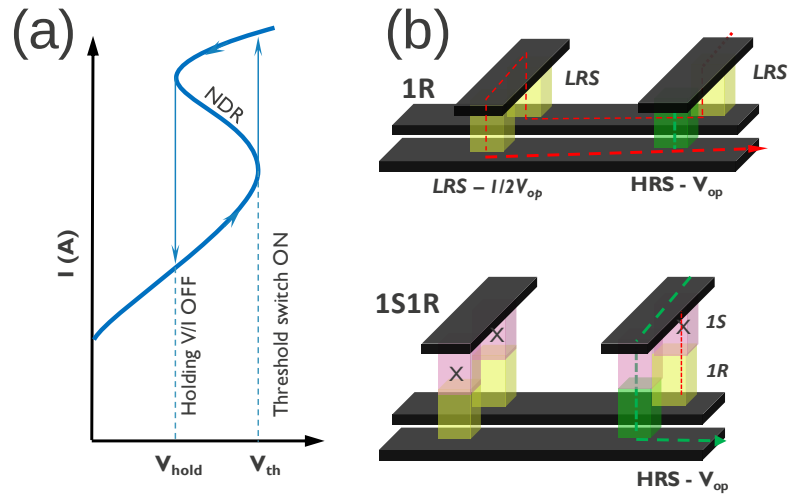

Figure 2 (a) OTS mechanism and the resulting Negative Differential Resistance provides a strong rectification. (b) A 2-terminal selector device set in series with a resistive element helps suppressing the parasitic leakage.

The present work is focusing on understanding the fundamental factors driving the volatile Ovonic threshold switches (OTS),[3, 4] which is the mechanism behind the negative differential resistance (NDR) observed in GeSe based chalcogenide materials, where at threshold, the leakage current increases exponentially with the NDR characteristic snap-back. On the downtrace and below a certain current level, the material stops conducting, therefore switching to an OFF state (Figure 2a).[3]

At the material level, the OTS mechanism is believed to be predominantly an electronic switching mechanism that relies on traps lying in the mobility-gap of the amorphous material that, upon the application of a critical electric field (*i.e.*, at V_{th}), become charged, change their

position with respect to the conduction/valence mobility edges and contribute to a significant current increase.[5, 6] Another description of the threshold switching considers the formation of an unstable filament that electrically shunts the selector material between the electrodes.[7, 8] The above-mentioned switching models are offering a consistent picture in the sense that the dominant component is driven by an electronic switching mechanism associated with picosecond range switching times,[9] and inter-trap distances and occupations that are used as fitting parameters.[10] On top of that, the dynamic response of the Ge/Se atoms might play an important role in the dielectric response, as witnessed for the *metavalent* bonds present in similar chalcogenide materials.[11, 12] The OTS mechanism is classically considered to be purely electronic in nature, but we do not exclude that the dynamics of the formed/broken bonds can have a great impact on the OTS mechanism. Bond dynamics, in turn, impact on the evolution of the atomic potential energy surface during the cycling of the device.

In large devices, a filamentation process was reported,[13] but the nature of the filamentation that can take place in nm-sized devices remains elusive, since the reported defect density, of the order of 10^{19} cm^{-3}, corresponds only to the response of a handful of electrically-active defects active across the device.[14] Historically, these traps were usually associated with the signature of a chalcogen lone-pair (LP) or of a valence-alternating-pair (VAP).[15] As we will show in this work, that is not always the case, especially for chalcogen-poor (and hence Ge-rich) materials, such as amorphous $Ge_{50}Se_{50}$ ($aGe_{50}Se_{50}$). This Se-poor composition (poor with respect to $GeSe_2$ stoichiometry) has almost all its Se atoms bonded to Ge ones and has hence a low probability to form Se VAP. Germanium, however, is abundant, and can hence form Ge-Ge states that lie in the mobility-gap, as reported in several first-principles studies.[3, 14, 16, 17]

Through this paper, we aim not only contributing to the building of a fundamental understanding of the atomic nature of the traps responsible for the OTS, how they evolve with the stoichiometry of the materials but more importantly, what are the inherent limitations bound

to the size of the atomistic models, typically used in theoretical approaches. Also, we investigate the influence of an electric field on those mobility-gap states before any atomic movement occurs.

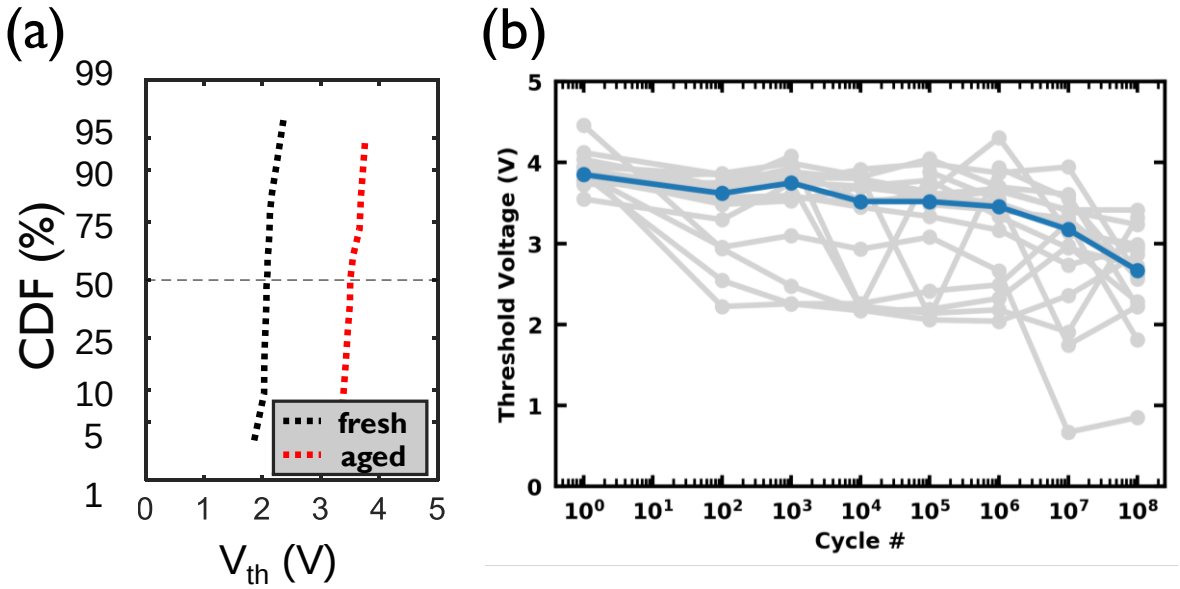

Figure 3 (a) V_{th} statistics in aGeSe drifts from initial 2V towards 3.5V after low-energy voltage-accelerated ageing. (b) High-energy pulsed-cycling drifts the V_{th} to lower voltages. Reprinted from [16], Copyright (2019), with permission from Elsevier

Furthermore, there is a great interest in understanding the ageing effects on the V_{th} instability, which is a big reliability issue: the voltage at which the materials switch ON should be stable/repeatable for billions of cycles. In practice, some materials can have significant V_{th} drift. Depending on the operating voltage and time, the same material can have two intrinsic degradation modes: at low energy stress (below average V_{th}, 3V / 100ns), the V_{th} drifts up in voltage (**Figure 3**a), whereas high energy stress/cycling (above average V_{th}, 5V / 100ns) tests show the V_{th} to drift to lower voltages (Figure 3b).[16, 18] The two different modes need to be understood so that the degradation can be alleviated.

The threshold switching process also takes place in phase-change memory chalcogenides before the crystallization,[6] supplying the material with the required Joule heating. In the selector devices, however, the crystallization process is undesired, since it will lead to memory switch, instead of volatile switch. The OTS behavior, characteristic of the amorphous state, is required

to be maintained for billions of cycles. On that front, a good thermal robustness (no crystallization/ageing during deposition or long operation cycles) of the selector material is the first criterium to meet.

In this account we present a detailed investigation of the electronic properties, unveil the nature of the charge traps in the mobility-gap of the amorphous materials for several Ge:Se ratios. The interaction of the electronic states in the mobility-gap with the electric field is presented. We show the possible consequences of the ageing process on the threshold voltage degradation mechanisms. Finally, we present a way to modulate the qualitative bonding in the material, therefore changing the electronic properties (current /voltage parameters) of the selector device.

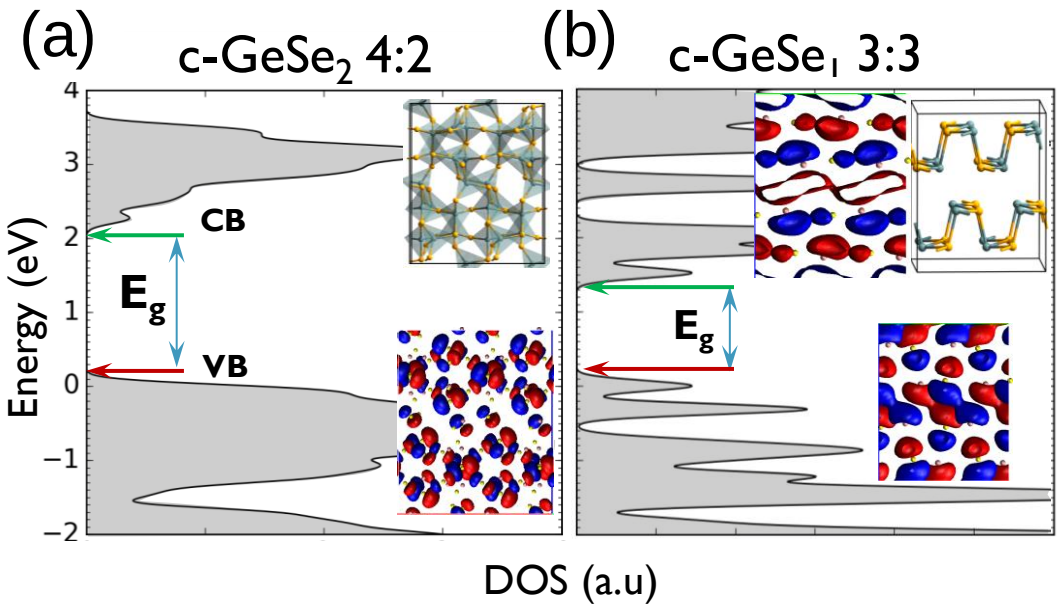

Figure 4: (a) Density of States in a $GeSe_2$ and (b) $GeSe_1$ crystalline phases. E_g – band gap, VB-Valence band (predominantly Se LP 4p free electron lone-pair), CB-Conduction band (predominantly DB-Ge $4sp^3$ hybrid orbital). Reprinted, with permission, from [3] Copyright 2017, IEEE.

Electronic structure: before diving into the electronic structure of the disordered systems, we first analyze in the **Figure 4**a and b the band gap of the crystalline $GeSe_2$ and $GeSe_1$ materials: $GeSe_2$ is a tetrahedrally bonded crystal, where the valence band (VB) is defined predominantly by the Se lone-pairs and the band gap is almost 50% wider than that of $GeSe_1$ crystal. In the

$GeSe_1$ there are only triply coordinated elements, which results in the sp^3 hybridized orbitals of Ge combining together to form the conduction/valence bands. (Figure 4b). Comparing the two crystalline cases, one can anticipate that non-tetrahedrally coordinated Ge will participate in the mobility-gap states/edges of the disordered materials, whenever present.

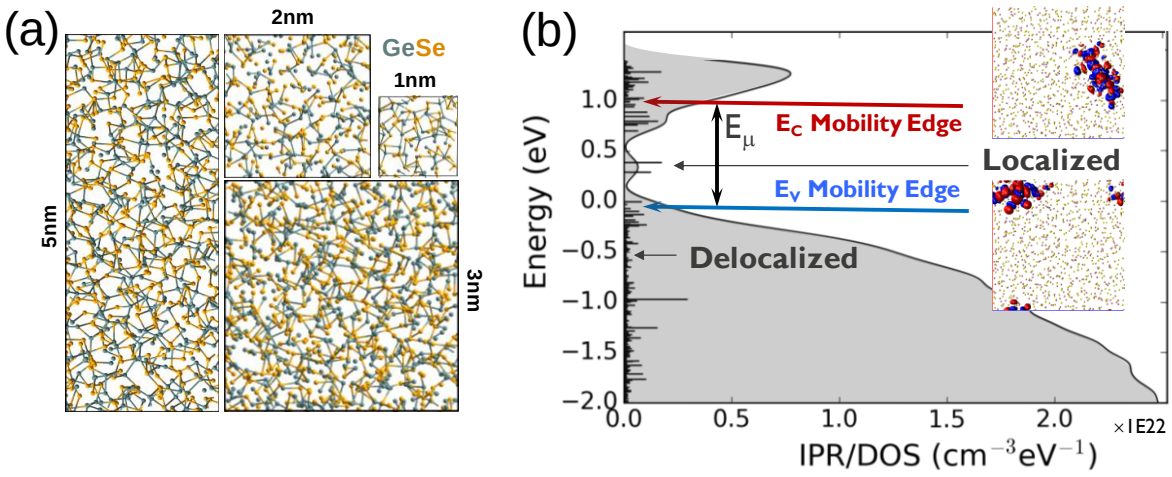

Figure 5 (a) Several model sizes were used for amorphous systems, ranging from 1 to 5 nm size (up to 1000 atoms) (b) typical DOS in amorphous GeSe chalcogenide materials: IPR – degree of localization, E_μ - mobility gap on a 3x3x3nm sample.

In the amorphous / disordered materials (model generation and structural details given in *Supporting Information*), the linear combination of atomic orbitals for a specific state will not span across all atoms of that model. Some states are localized in space (Anderson localization) and conduction through those states will be slower, if compared to the conduction through a crystal band. To identify the state localization, we tested several model sizes (**Figure 5**a) and the Inverse Participation Ratio (IPR) is computed for each state: the high values are characteristic of highly localized state.[19] As for the electronic properties, in the amorphous materials we look for the mobility gap (E_μ) and the span of mobility edge tails (near conduction and valence edges), which consist of localized states (Figure 5b).

In the **Figure 6**a, we depict a highly delocalized state of a 1x1x5nm model, which is usually at or below/above the valence/conduction mobility edges. Between the mobility edges, we have localized states (Figure *6*b,c). If the localization length (*i.e.*, span in space of > 99.9% electronic

density of the localized state) is larger than the model size, that localized state can be artificially detected as delocalized, therefore mobility gap extraction has to suffer: the state in Figure 6b artificially seems to be delocalized in the short cell dimension directions. Apart from the exchange-correlation functional corrections that are needed to the GGA-DFT treatment, it is important that the model size is large enough not to introduce this type of artefacts in the detection of the mobility gap. We extracted a localization length in the range of 1.5-3nm (trap concentration of 10^{19}-10^{20} cm^{-3}) and concluded that a minimum model size of 2nm is required to investigate the electronic properties of chalcogenides under study.

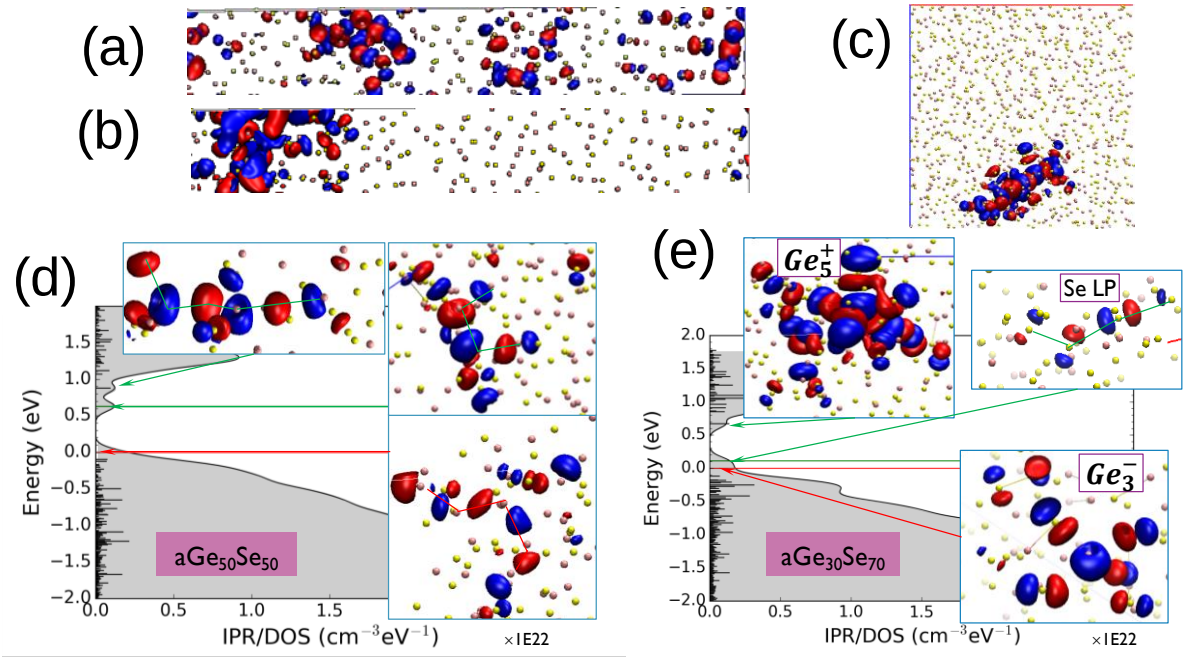

Figure 6 (a) A typical delocalized state in 1x1x5nm amorphous GeSe model (iso-surface representations) (b) state that is localized in the longitudinal direction of the model but delocalized in the other two directions. (c) fully localized state in a 3x3x3nm (d) Typical DOS in 2x2x2nm Ge-rich $aGe_{50}Se_{50}$ model with few representations of Ge-Ge gap/tail states as insets. Reprinted from [16], Copyright (2019), with permission from Elsevier (e) Typical DOS in Se-rich $aGe_{30}Se_{70}$ model with few Se-LP, Ge_3^-/Ge_5^+ VAP gap/tail states representations as insets.

Figure 6d shows typical DOS of Ge-rich $aGe_{50}Se_{50}$ 3x3x3nm model, with localized states between the mobility edge states that show the nature of the gap states: predominantly the trapping states are formed of Ge-Ge "chains" with small contributions from Se LP. The same Ge-Ge bonds were found in am-GeTe.[20] In the case of a Se-rich stoichiometry ($aGe_{30}Se_{70}$

Figure 6e), we could witness a different picture: Se abundance leads to states that are made of Se LP near the valence edge, whereas conduction tail-states show strong Ge contribution. On a close inspection, we concluded that their nature can be described as VAP of Ge (under- and over-coordinated Ge, see details in *Supporting Information*), even though the two states are spatially far from each-other (see **Figure 7**). In other words, not only in chalcogens but also in Ge there can form valence-alternating pairs that can trap electrons/holes and contribute to the Ovonic threshold switching mechanism. A detailed description of the coordination environments in these chalcogenides was given by Raty *et al.*,[12, 21] whereas Li and Robertson showed the qualitative n-type nature of the traps in Ge-rich compositions.[14]

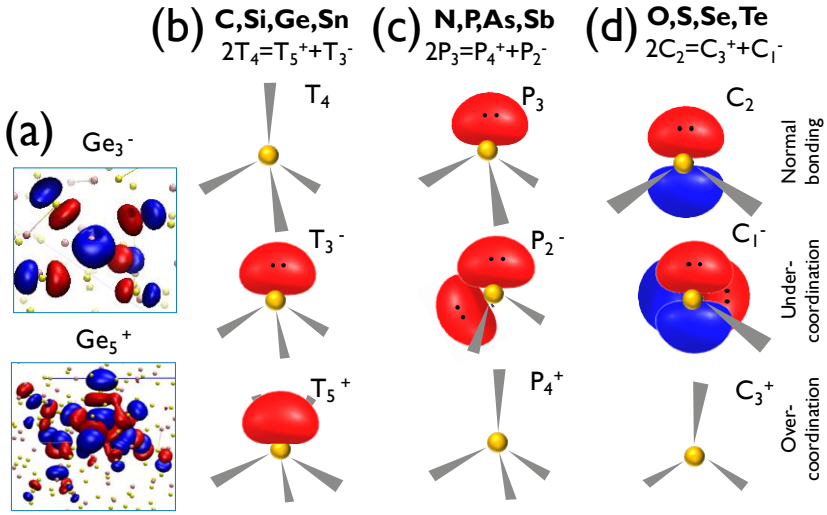

Figure 7 (a) VAP states observed in Ge shown for under- and over- coordinated Ge atoms in $aGe_{30}Se_{70}$. The corresponding coordination configurations are depicted for (b) tetragens, (c) pnictogens and (d) chalcogens. Reprinted from [16], Copyright (2019), with permission from Elsevier

Since we deal with disordered materials, there are an infinite number of possible atomic morphologies of the modeled system, hence we need a statistical evaluation of the mobility gaps, extracted from the density of states (DOS). **Figure 8**a presents the DOS for 10 different models that were aligned at the valence edge of the mobility gap, whereas in Figure 8b the statistical boxes for several Ge:Se stoichiometries (10 models each) are shown.

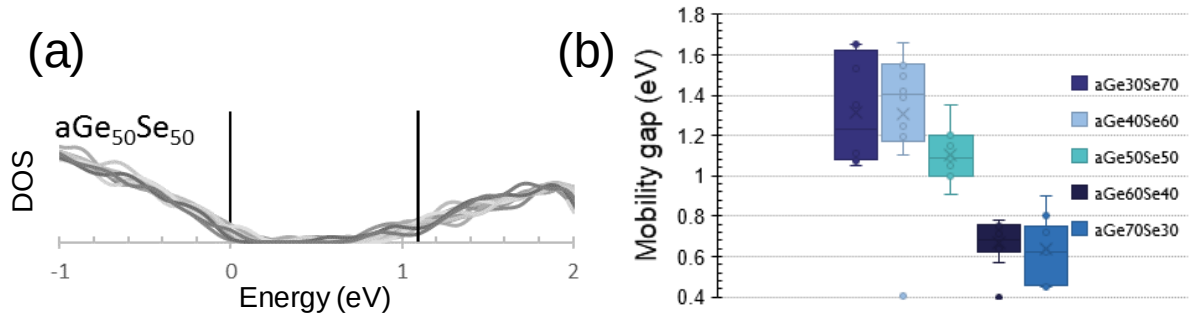

Figure 8 (a) Density of States for 10 models of 2x2x2nm $aGe_{50}Se_{50}$ (b) Mobility gaps (statistical boxes for 10 models each) for aGe_xSe_y (x:y=30:70,40:60,50:50,60:40,70:30)

With Ge approaching 60%, the mobility gap of the GeSe chalcogenide approaches the gap of pure Ge: Ge-related states are omnipresent and define the mobility edges and gap traps. Photoconductivity experiments on similar stoichiometries (Ge 40-60%) show that the mobility gap is similar in all cases and close to the direct gap of Ge - 1.05eV (**Figure 9**).

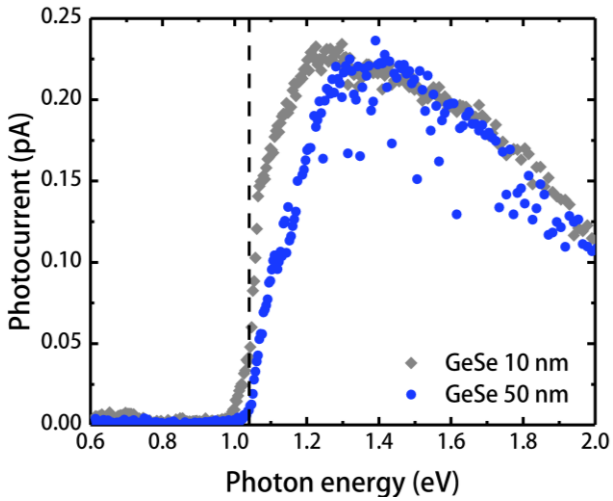

Figure 9 (a) Experimental determination of GeSe bandgap in $aGe_{64}Se_{36}$ layers from the onset of photoconductivity current.

The mobility edges we extracted from IPR analysis (detailed in *Supporting Information*) represent the electrically conducting states within the valence/conduction bands, which could be the source of discrepancy with photoconductivity measurements, where an optical absorption precedes the conductivity. The mobility gap of the Se-rich compositions (1.2-1.6 eV Figure 8b) approaches the band gap of the perfect crystalline $GeSe_2$ (Figure 4b).

Electric field: the interaction of the electric field with the electronic states can reveal how much of the purely electronic component in the OTS mechanism is effective – the ionic component (upon atomic relaxation) can have a great impact on the electronic wavefunction of the system, therefore we isolate any ionic/polaronic relaxation effects by keeping the atoms fixed. To illustrate the effect, we applied a uniform electric field across a 2x2x5nm model of $aGe_{50}Se_{50}$. The electric field interaction (change in energy and degree of localization) is show in **Figure 10**. For some states there is a stronger Stark effect[22] and their energy drops/raise in energy faster than for other states (Figure 10a), resulting in wider conduction/valence tails at high fields, effectively shrinking the mobility gap.[3] In high electric fields (0.8V/nm) the tails become so close that electronic excitation from valence to conduction states occurs and that leads co convergence issues. Electric field interaction is not uniform in space neither: some regions are more readily to intermix with tail states than other regions in space, which illustrates the electronic structure inhomogeneities in the disordered chalcogenide materials.

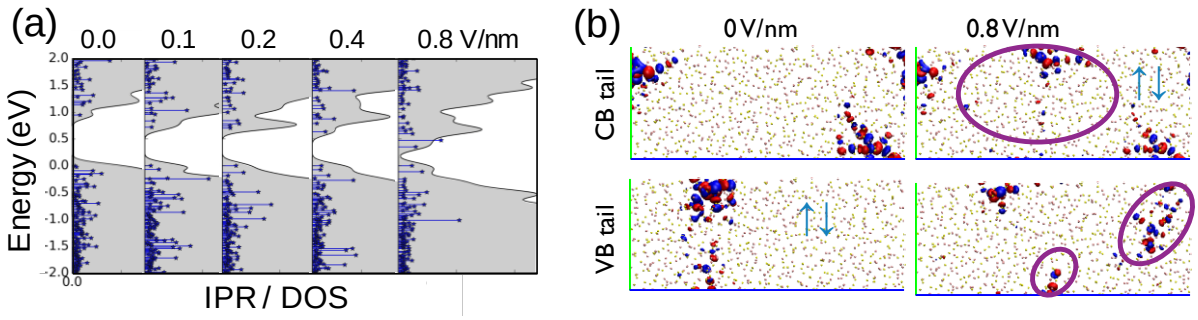

Figure 10. (a) Influence of the electric field on the DOS for a 2x2x5nm $aGe_{50}Se_{50}$ sample. (b) Illustration of qualitative changes of one valence and one conduction tail states, under applied electric field of the same sample. Arrows indicate electronic occupation; ovals highlight the delocalization to other regions of the model. Reprinted, with permission, from [3] Copyright 2017, IEEE.

Figure 10b illustrates state delocalization to an island of atoms in the neighborhood and the corresponding electronic excitation. These changes (tail/mobility gap states (de)localization in space change the spatial span of the electronic gap states) will result in changes of the electric conductivity of the material. This is consistent with the field-induced edge state delocalization model.[8]

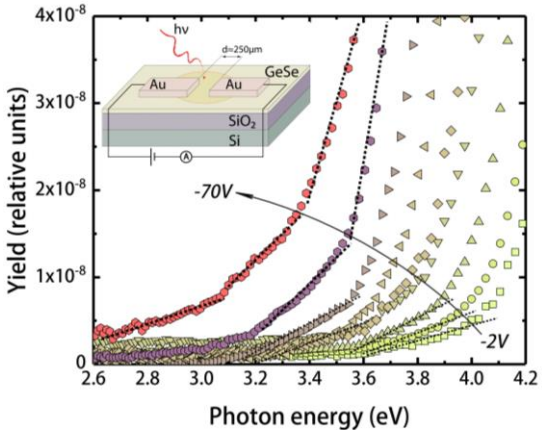

Figure 11. (a) Gap/tail state evolution upon varying electric field from IPE spectroscopy on a Si\SiO_2\aGeSe\Au device.

The experimental evolution of the tail states under applied electric field was measured on a thin film of $aGe_{50}Se_{50}$, deposited on SiO_2 (**Figure 11**). The slope of the onset of the Internal Photo-emission (IPE) spectra evolves upon increased bias,[23] indicating a "spill out" of the band tail states into the mobility gap with increasing electric field, as predicted by the theoretical calculations (Figure 10a). However, since in the experimental measurement the ionic/polaronic relaxation effects are included, the contribution from purely electronic component is not quantifiable.

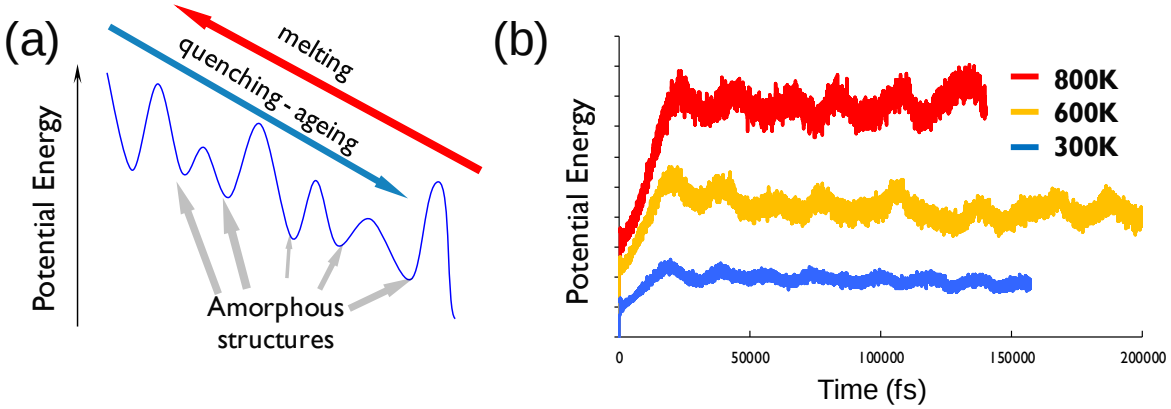

Figure 12 (a) Amorphous phase locked in a local minimum can drift downwards during ageing or upwards during melting (b) AIMD simulations of a 2x2x2nm aGeSe sample show different slopes at different temperatures for the potential energy trajectory of the material. Reprinted from [16], Copyright (2019), with permission from Elsevier

Ageing: if the crystalline materials are stable in time and the atoms only vibrate around a certain equilibrium position, in disordered materials the atomic conformations are kinetically arrested in a high-energy local minimum. This high potential energy of the atomic configuration,

compared to the crystalline counterpart, is intrinsic to the amorphous materials. The potential energy surface is very rich in local minima and there is a thermodynamic driving force towards lower-energy conformations. If the system does not exceed the melting threshold (glass-transition temperature for aGeSe is 568K[24]), the thermal energy is just large enough to promote atomic movements over small kinetic barriers. The system continuously rearranges the atomic bonding, the material's morphology evolves in time towards an energetically more stable atomic configuration. The rate of this energy relaxation process (ageing), depends on the kinetic energy speedup. On excess kinetic energy, the material is melting (**Figure 12**a).

To obtain a qualitative insight into the ageing/melting processes, we performed AIMD simulations of the $aGe_{50}Se_{50}$ system at different temperatures (Figure 12b). Low kinetic energy (300K) conditions show a rather fast equilibration of the atomic configuration and not much of energy drift (flat average slope). Increasing the vibrational kinetic energy to 600K allows for jumps over larger barriers and further stabilization of the system, which can be observed as a negative average slope of the potential energy trajectory. Increasing the kinetic energy to 800K, the system seems to be capable to jump over larger barriers to reach the thermal equilibrium. A positive average slope of the trajectory would point towards material melting. Ignoring the melting regime, a greater interest is what happens with the disordered material during the ageing. As evidenced in the previous sections, the Ge "chains" or clusters are responsible for the electrical behavior of this material. Therefore, we considered the Ge-Ge bond concentration as an indirect metric for the evolution of the mobility-gap charge traps and monitored its evolution during the span of the Ab Initio Molecular Dynamics (AIMD) simulation. In **Figure 13** we monitor the amount of Ge-Ge bonds in time. Starting at a level of 23%, the amount of Ge-Ge bonds quickly drops below 15% after 50ps at 600K. Of course, this relaxation time depends on the simulated temperature; at room-temperature the Ge-Ge bond reduction evolves much slower than at higher temperatures and we speculate that this mechanism is the main contributor to the

ageing of the intrinsic electrical signature (drift of V_{th} in Figure 3) of the $aGe_{50}Se_{50}$ selector.[16] The decrease of Ge-Ge homopolar bonds happens because the bonds like Ge-Ge or Se-Se are thermodynamically less stable/exothermic than Ge-Se bonds in aGeSe (in other words non-preferred) as illustrated by the evolution of the short-range order coefficient, which represents the departure from the complete chemical disorder in the amorphous materials (Figure 13b).[25] Therefore, they have the tendency to disappear or at least to reduce their concentration, compensated by an increase of heteropolar (more exothermic) Ge-Se bonds.

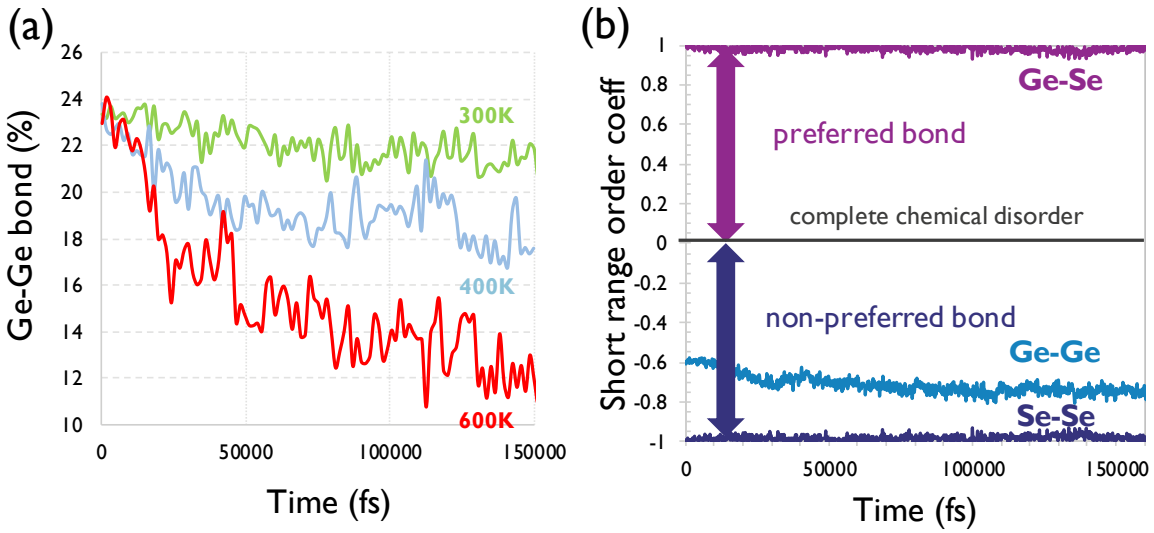

Figure 13 (a) AIMD evolution of Ge-Ge bond % in time with ageing at different temperatures for the 2x2x2nm sample. (b) Short range order coefficients computed on the atomic trajectory at 600K for the same 2x2x2nm sample– amount of Ge-Ge bonds is reduced.

This mechanism represents the thermodynamic driving force for ageing of the material. A decrease in Ge-Ge-derived trap states would increase the mobility gap of the material, as illustrated on few potential-energy-minimum points on the AIMD trajectory (**Figure 14**): ageing of the material results in a decrease of Ge-Ge bonds and an increase of the mobility gap. The exact same mechanism was shown to be responsible for the ageing in GeTe,[17] hence it is general for disordered Ge chalcogenides. If during the first-fire event the required amount/configuration of traps and the mobility gap is defined with the initial V_{th} of OTS, their

further evolution in time with two opposite mechanisms (ageing or melting, depending on the energy injected in the material) will determine the V_{th} to drift upwards or downwards.

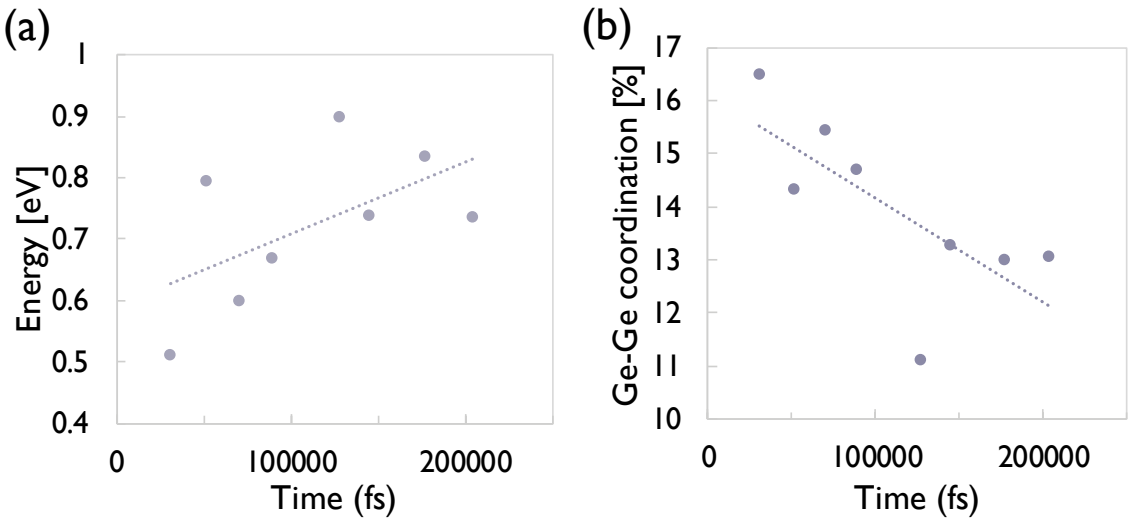

Figure 14 a) Mobility gap E_{μ} increases in time, which correlates with b) a decrease in Ge-Ge bonds in the 2x2x2nm $aGe_{50}Se_{50}$ sample.

This type of ageing was also observed in other IV-VI compounds. [16, 18, 21] In other words, the Ge-Ge bond temporal instability constitutes a reliability issue and is the most probable cause for the threshold voltage drift. However, the proposed model does not preclude other possible contributions such as the extent to which the trap relaxation depends on the captured charge and its impact on the resulting threshold switching process.

Si/N doping: Doping with atoms that introduce strong bonds in the system strengthens the atomic matrix against element diffusion. This increases the thermal robustness of the selector materials in excess of 400°C, as shown by in-situ XRD measurements on Si/N:$aGe_{50}Se_{50}$ (**Figure 15**).[3] The impact of Si doping on the crystallization temperature is weaker, compared to N doping. Thermal properties improvement upon N doping have been shown for Se-rich aGeSe as well.[26]

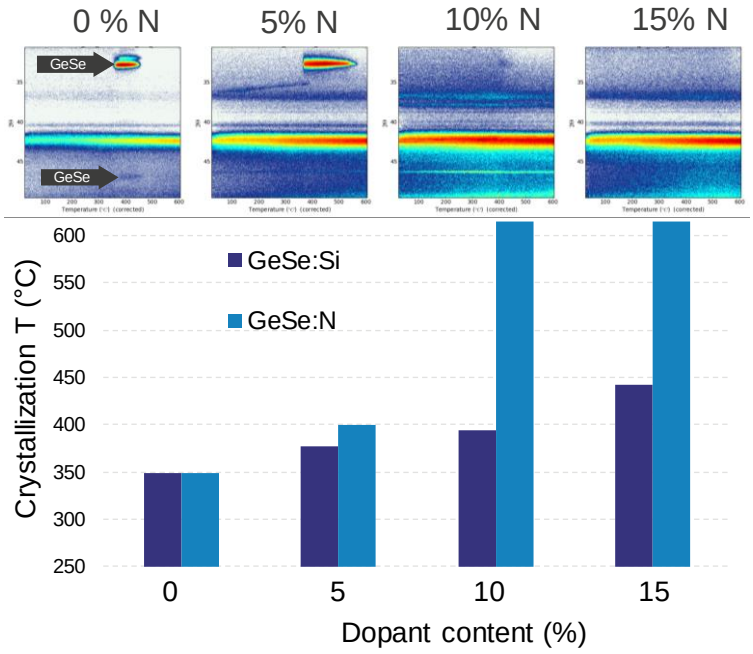

Figure 15: In-situ XRD thermal stability of Si/N:a$Ge_{50}Se_{50}$ shows increase of the crystallization temperature with the dopant content. Reprinted, with permission, from [3] Copyright 2017, IEEE.

Considering the different nature of the Si and N atoms, it is interesting to see what type of changes in terms of bonding are induced into aGeSe material by Si or N doping. In that respect, Si, Ge are less electronegative and N, Se are more electronegative elements. As a result, Ge coordination analysis shows that Ge-N bonds replace both Ge-Ge and Ge-Se bonds, whereas Si-Ge bonds replace mostly Ge-Se bonds (**Figure 16**).

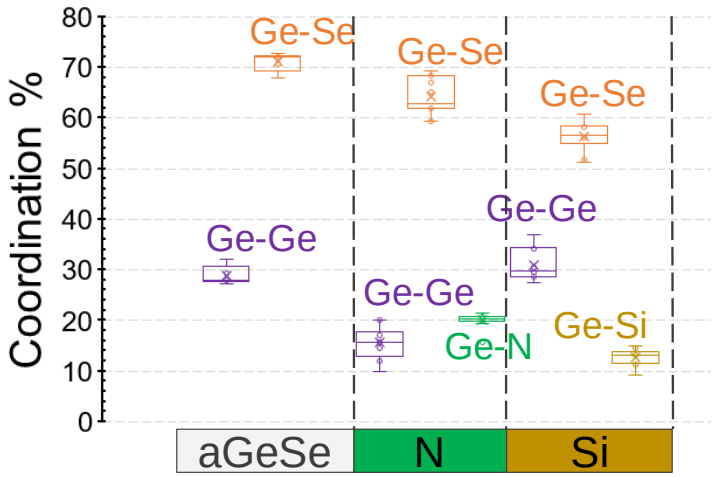

Figure 16: Amount of Ge coordination with Ge, Se, N or Si in small (~1x1x1nm-sized models) of Si/N:a$Ge_{50}Se_{50}$. Reprinted, with permission, from [3] Copyright 2017, IEEE.

Since the Ge-Ge homopolar bonds were found to constitute mobility-gap states, reducing their amount by N doping results in fewer traps and wider/cleaner mobility-gap, as shown in **Figure 17**a for a set of 10 small 100-atoms models. This leads to the conclusion that N doping can reduce the leakage, which was also witnessed in other chalcogen materials.[27] Indeed, experimental *I-V* measurements on increasing N concentration in splits with similar Ge:Se composition shows leakage reduction in large area MIM capacitors (Figure 17b). Therefore, a low concentration of gap states reduces the I_{OFF} leakage/increases the half-bias nonlinearity at the expense of increased mobility-gap, therefore of threshold voltage. A negative consequence is that during switching cycling, the N-doped material undergoes higher energy stress compared to the undoped one and a larger drift of threshold voltage. While the N-doping strategy was shown to bring electrical, stability improvements in many chalcogen materials/devices,[28] it does not alleviate the V_{th} drift issue in GeSe selector device.[29]

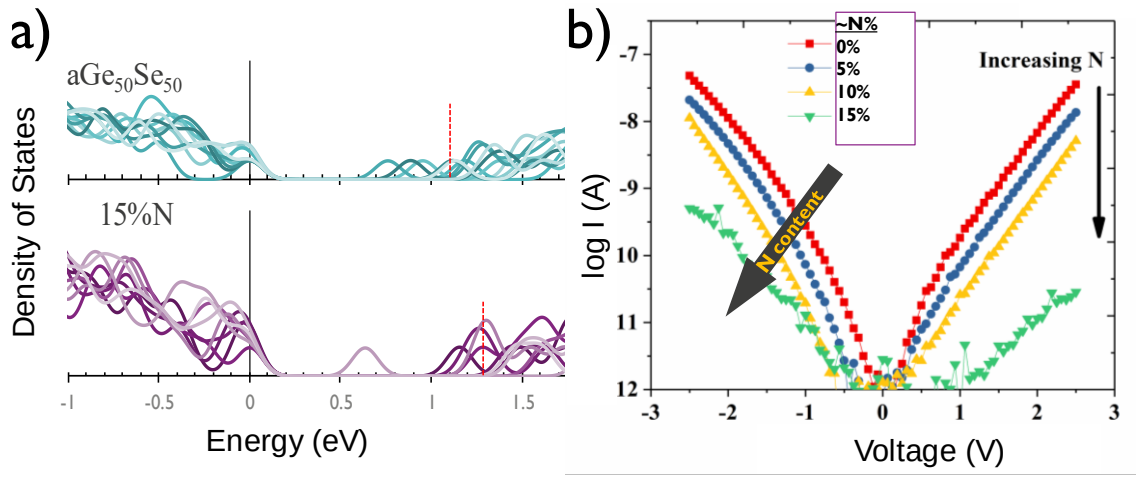

Figure 17: (a) Density of States for 10 amorphous models of undoped and N:$aGe_{50}Se_{50}$ (small ~1x1x1nm samples) (b) Current-Voltage traces for 0-15% N doping levels. Reprinted, with permission, from [3] Copyright 2017, IEEE.

Conclusions: We show that the nature of the mobility gap conductive defects in GeSe-based (Ge-rich) selector materials is predominantly of Ge nature (Ge-Ge "chains"/clusters), whereas in Se-rich compositions, the electronic structure of aGeSe show the possibility to have Valence Alternating Pairs of Ge states. We found that next to a more accurate hybrid DFT approach, a

minimum sized atomistic model is required to detect an accurate mobility gap of amorphous chalcogenides. The sole effect of electric field is enough to promote both an electronic re-population and state intermixing, therefore changing the electrical conduction (the localization length of the gap states/the inter-trap distance/ electron mobility) of the material. The observed modulation of the electronic structure with the applied electric field is supported by photoemission spectra measurements. AIMD simulations show that the thermodynamically unfavorable Ge-Ge bonds are not stable in time, also confirmed with RAMAN experiments. Hence the trap concentration in the mobility gap have the tendency to change in time. This can explain the long-term evolution of the threshold voltage in Ge-rich GeSe selector materials. To increase the melting/glass transition temperature, admixture with strong covalent-bonding elements is required. N-doped devices show a two-fold improvement: an increase in thermal stability, at the same time I_{OFF} leakage current drops, as expected from first-principles simulations results. Doping, however, did not improve on the V_{th} drift.

Experimental Section

Experimental samples preparation: integration performed in a 300nm process flow as Metal-Insulator-Metal selector devices with amorphous chalcogenide films with thickness varying from 5 to 20 nm, that have been deposited by physical vapor deposition (PVD) technique.[30] Amorphous GeSe films are prepared by room temperature physical vapor deposition (PVD). TiN/aGeSe/TiN selector devices were integrated in a 300nm process flow, using a pillar (TiN) bottom electrode, passivated with a low-temperature BEOL process scheme. A GeSe chalcogenide films control down to 5nm thickness has been achieved. N-dopants have been introduced by turning on a N_2 flow in the PVD chamber during the deposition process. Dynamic I-V characteristics were collected with an oscilloscope, monitoring the device response to a triangular pulse (equal fall/rise time of 100ns). Photoemission measurements under high applied electric field were performed on aGeSe films deposited on SiO_2 with evaporated Au

dots on top. Thermal stability in-situ XRD measurements were performed with a rate of 0.2 degree/s.

Computational methodology: Theoretical (Density Functional Theory) simulations were carried out in CP2K,[31] employing Goedecker, Teter and Hutter pseudo-potentials[32] and localized basis sets (of Double-Zeta-Valence-Polarization quality) in the Generalized Gradient Approximation (Perdew-Burke-Ernzerhof exchange-correlation functional[33]) for the melt-and-quench algorithm to generate the amorphous models. Several sizes were used for different purposes, ranging from 1nm to 5nm large models (Figure 5a): small (1nm) models we use to illustrate the minimum requirements on the model size for quantitative electronic structure simulations, long (5nm) models were used in electric field simulations, whereas the 2-3nm models are optimal to investigate the electronic properties. For the melt-and-quench protocol, a 3-temperature steps algorithm was employed, in which the models were melted at 1200K , then quenched at 800K and 400K with a fast pressure-release step (3 iterations of cell relaxation) between quenching steps. Computational time was determined, based on the total energy evolution of the system - every 3ps the average total energy compared to the previous run and the temperature step run stopped when the average total energy difference fell under 3eV. With such an algorithm, the melting time for 2x2x2nm models was 15-24ps, quenching at 800K and 400K typically lasted 6ps each for a total melt-and-quench time of 27-36ps. The small 1x1x1nm models reached the given threshold faster, total time typically 12-15ps. As a final step , a full system relaxation was performed. With an Ab-Initio Molecular Dynamics (AIMD) approach, we investigated the time evolution in a 2x2x2nm model – ageing, material relaxation / drift of the bonding. For the AIMD simulations, a Nosé thermostat was used.[34] A hybrid method (HSE functional[35]) in combination with the Auxiliary Density Matrix Method (ADMM) was used to quantify the electronic structure on 10 samples of 2x2x2nm size,[36] results were similar on a 3x3x3nm sized model. IPR for each state in the amorphous model was

used to define the edges for the mobility gap (see *Supporting Information* for details). A subsequent hybrid HSE functional relaxation on a sample system showed insignificant structural changes in the atomic model. Computations with a finite periodic electric field were performed by using the Berry-phase approach.[37]

Acknowledgements

This work was carried out in the framework of the imec Core CMOS – Emerging Memory Program. Financial support from EU H2020-NMBP-TO-IND-2018 project "INTERSECT" (Grant No. 814487) is acknowledged.

Received:

Revised:

Published online:

References

[1] http://www.itrs2.net/, accessed: September, 2017; G. W. Burr, R. S. Shenoy, K. Virwani, P. Narayanan, A. Padilla, B. Kurdi, H. Hwang, *Journal of Vacuum Science & Technology B* **2014**, 32, 040802.

[2] A. Chen, *Journal of Computational Electronics* **2017**, 16, 1186.

[3] S. Clima, B. Govoreanu, K. Opsomer, A. Velea, N. S. Avasarala, W. Devulder, I. Shlyakhov, G. L. Donadio, T. Witters, S. Kundu, L. Goux, V. Afanasiev, G. S. Kar, G. Pourtois, presented at IEEE International Electron Devices Meeting (IEDM) **2017**.

[4] H. Y. Cheng, W. C. Chien, I. T. Kuo, C. W. Yeh, L. Gignac, W. Kim, E. K. Lai, Y. F. Lin, R. L. Bruce, C. Lavoie, C. W. Cheng, A. Ray, F. M. Lee, F. Carta, C. H. Yang, M. H. Lee, H. Y. Ho, M. BrightSky, H. L. Lung, presented at IEEE International Electron Devices Meeting (IEDM) **2018**; G. C. Vezzoli, P. J. Walsh, M. A. Shoga, *Philosophical Magazine B* **1991**, 63, 739; S. Hudgens, *Physica Status Solidi B-Basic Solid State Physics* **2012**, 249, 1951.

[5] A. Calderoni, M. Ferro, D. Ielmini, P. Fantini, *Ieee Electron Device Letters* **2010**, 31, 1023; D. Ielmini, Y. G. Zhang, *Journal of Applied Physics* **2007**, 102, 054517; D. Ielmini, *Physical Review B* **2008**, 78, 035308; W. Czubatyj, S. J. Hudgens, *Electronic Materials Letters* **2012**, 8, 157; A. Pirovano, A. L. Lacaita, A. Benvenuti, F. Pellizzer, R. Bez, *Ieee Transactions on Electron Devices* **2004**, 51, 452.

[6] A. Redaelli, A. Pirovano, A. Benvenuti, A. L. Lacaita, *Journal of Applied Physics* **2008**, 103, 111101.

[7] I. V. Karpov, M. Mitra, D. Kau, G. Spadini, Y. A. Kryukov, V. G. Karpov, *Journal of Applied Physics* **2007**, 102, 124503; V. G. Karpov, Y. A. Kryukov, I. V. Karpov, M. Mitra, *Physical Review B* **2008**, 78, 052201.

[8] M. Nardone, M. Simon, I. V. Karpov, V. G. Karpov, *Journal of Applied Physics* **2012**, 112, 071101.

[9] F. Buscemi, E. Piccinini, A. Cappelli, R. Brunetti, M. Rudan, C. Jacoboni, *Applied Physics Letters* **2014**, 104, 022101; M. Wimmer, M. Salinga, *New Journal of Physics* **2014**, 16, 113044.
[10] M. Kaes, M. Salinga, *Scientific Reports* **2016**, 6, 31699.
[11] J. Y. Raty, M. Schumacher, P. Golub, V. L. Deringer, C. Gatti, M. Wuttig, *Advanced Materials* **2019**, 31, 1806280; M. Wuttig, V. L. Deringer, X. Gonze, C. Bichara, J. Y. Raty, *Advanced Materials* **2018**, 30, 1803777.
[12] J. Y. Raty, P. Noe, presented at E\PCOS **2019**.
[13] K. E. Petersen, D. Adler, *Journal of Applied Physics* **1979**, 50, 5065.
[14] H. L. Li, J. Robertson, *Scientific Reports* **2019**, 9, 1867.
[15] M. Kastner, D. Adler, H. Fritzsche, *Physical Review Letters* **1976**, 37, 1504.
[16] S. Clima, D. Garbin, W. Devulder, J. Keukelier, K. Opsomer, L. Goux, G. S. Kar, G. Pourtois, *Microelectronic Engineering* **2019**, 215, 110996.
[17] S. Gabardi, S. Caravati, G. C. Sosso, J. Behler, M. Bernasconi, *Physical Review B* **2015**, 92, 054201.
[18] S. Clima, D. Garbin, W. Devulder, J. Keukelier, K. Opsomer, L. Goux, G. S. Kar, G. Pourtois, presented at INFOS **2019**.
[19] J. J. Dong, D. A. Drabold, *Physical Review Letters* **1998**, 80, 1928.
[20] F. Zipoli, A. Curioni, presented at *E/PCOS* **2013**; A. V. Kolobov, P. Fons, J. Tominaga, *Scientific Reports* **2015**, 5, 13698.
[21] J. Y. Raty, W. Zhang, J. Luckas, C. Chen, R. Mazzarello, C. Bichara, M. Wuttig, *Nature Communications* **2015**, 6, 7467.
[22] P. S. Epstein, *Physical Review* **1926**, 28, 695.
[23] V. V. Afanas'ev, *Advances in Condensed Matter Physics* **2014**, 301302.
[24] J. Pries, S. Wei, M. Wuttig, P. Lucas, *Advanced Materials* **2019**, 31, 1900784.
[25] I. Pethes, R. Chahal, V. Nazabal, C. Prestipino, A. Trapananti, S. Michalik, P. Jovari, *Journal of Physical Chemistry B* **2016**, 120, 9204.
[26] A. Verdy, G. Navarro, V. Sousa, P. Noe, M. Bernard, F. Fillot, G. Bourgeois, J. Garrione, L. Perniola, presented at IEEE International Memory Workshop (IMW) **2017**.
[27] A. Verdy, F. d'Acapito, J. B. Dory, G. Navarro, M. Bernard, P. Noe, *Physica Status Solidi-Rapid Research Letters* **2019**, 1900548.
[28] A. Verdy, F. d'Acapito, J. B. Dory, G. Navarro, M. Bernard, P. Noe, *Physica Status Solidi-Rapid Research Letters*; A. Fantini, V. Sousa, L. Perniola, E. Gourvest, J. C. Bastien, S. Maitrejean, S. Braga, N. Pashkov, A. Bastard, B. Hyot, A. Roule, A. Persico, H. Feldis, C. Jahan, J. F. Nodin, D. Blachier, A. Toffoli, G. Reimbold, F. Fillot, F. Pierre, R. Annunziata, D. Benshael, P. Mazoyer, C. Vallee, T. Billon, J. Hazart, B. De Salvo, F. Boulanger, Ieee, *2010 International Electron Devices Meeting - Technical Digest* **2010**; B. L. Huang, *Physica Status Solidi B-Basic Solid State Physics* **2015**, 252, 431; Y. F. Lai, B. W. Qiao, J. Feng, Y. Le, L. Z. La, Y. Y. Lin, T. A. Tang, B. C. Cai, B. M. Chen, *Journal of Electronic Materials* **2005**, 34, 176.
[29] N. S. Avasarala, G. L. Donadio, T. Witters, K. Opsomer, B. Govoreanu, A. Fantini, S. Clima, H. Oh, S. Kundu, W. Devulder, M. H. van der Veen, J. Van Houdt, M. Heyns, L. Goux, G. S. Kar, Ieee, presented at IEEE Symposium on VLSI Technology **2018**.
[30] B. Govoreanu, G. L. Donadio, K. Opsomer, W. Devulder, V. Afanasiev, T. Witters, S. Clima, N. S. Avasarala, A. Redolfi, S. Kundu, O. Richard, D. Tsvetanova, G. Pourtois, C. Detavernier, L. Goux, G. S. Kar, presented at IEEE Symposium on VLSI Technology **2017**.
[31] J. Hutter, M. Iannuzzi, F. Schiffmann, J. VandeVondele, *Wiley Interdisciplinary Reviews: Computational Molecular Science* **2014**, 4, 15.

[32] S. Goedecker, M. Teter, J. Hutter, *Physical Review B* **1996**, 54, 1703; M. Krack, *Theoretical Chemistry Accounts* **2005**, 114, 145.
[33] J. P. Perdew, K. Burke, M. Ernzerhof, *Physical Review Letters* **1996**, 77, 3865.
[34] S. Nose, *Journal of Chemical Physics* **1984**, 81, 511.
[35] J. Heyd, G. E. Scuseria, M. Ernzerhof, *Journal of Chemical Physics* **2003**, 118, 8207.
[36] M. Guidon, J. Hutter, J. VandeVondele, *Journal of Chemical Theory and Computation* **2010**, 6, 2348.
[37] I. Souza, J. Iniguez, D. Vanderbilt, *Physical Review Letters* **2002**, 89, 117602.

Density-Functional Theory investigations on amorphous Ge_xSe_y - based chalcogenides show that the mobility-gap trap states change their nature with Ge:Se ratio, applied electric field and ageing. Changes in mobility-gap trap concentration during selector device operation has a detrimental influence on the threshold voltage. Si/N doping strategy shows improvement in crystallization *T* and I_{OFF}.

Keyword chalcogenides, selector, DFT

Sergiu Clima, Daniele Garbin, Karl Opsomer, Naga S. Avasarala, Wouter Devulder, Ilya Shlyakhov, Jonas Keukelier, Gabriele L. Donadio, Thomas Witters, Shreya Kundu, Bogdan Govoreanu, Ludovic Goux, Christophe Detavernier, Valeri Afanas'ev, Gouri S. Kar, Geoffrey Pourtois*

Ovonic Threshold Switching Ge_xSe_y Chalcogenide Materials: Stoichiometry, Trap Nature and Material Relaxation from First Principles